J Solid State Electrochem (2009) 13:1273–1278
DOI 10.1007/s10008-008-0667-3

ORIGINAL PAPER

Electrochemical synthesis of Fe_3O_4-PB nanoparticles with core-shell structure and its electrocatalytic reduction toward H_2O_2

Jiang Chumming · Lin Xiangqin

Received: 24 June 2008 / Revised: 27 August 2008 / Accepted: 2 September 2008 / Published online: 21 September 2008

Abstract The Fe_3O_4-Prussian blue (PB) nanoparticles with core-shell structure have been in situ prepared directly on a nano-Fe_3O_4-modified glassy carbon electrode by cyclic voltammetry (CV). First, the magnetic nano-Fe_3O_4 particles were synthesized and characterized by X-ray diffraction. Then, the properties of the Fe_3O_4-PB nanoparticles were characterized by CV, electrochemical impedance spectroscopy, and superconducting quantum interference device. The resulting core-shell Fe_3O_4-PB-modified electrode displays a dramatic electrocatalytic ability toward H_2O_2 reduction, and the catalytic current was a linear function with the concentration of H_2O_2 in the range of 1×10^{-7}~5×10^{-4} mol/l. A detection limit of 2×10^{-8} ($s/n=3$) was determined. Moreover, it showed good reproducibility, enhanced long-term stability, and potential applications in fields of magnetite biosensors.

Keywords Fe_3O_4 · PB · Core-shell structure · Nanoparticles · H_2O_2

Introduction

Nanosized materials offer many advantages due to their unique size and physical properties. In recent years, magnetite (Fe_3O_4) nanoparticle, due to its good biocompatibility, strong superparamagnetic property, low toxicity, and easy preparation process, is becoming the focus of research and has attracted increasing attention in the fields of biology [1], microwave absorption [2], and sensors [3, 4]. The Fe_3O_4 nanoparticles can provide a favorable microenvironment for proteins to directly immobilize on the electrode surface, and the protein-Fe_3O_4 film illustrates good catalytic activity toward some biological or environmental molecules, such as hydrogen peroxide, trichloroacetic acid, etc. [5–8]. Reetz et al. [9] reported mechanically stable lipases-Fe_3O_4 nanoparticles sol-gel biocatalysts by simultaneous entrapment of lipase and nanostructured Fe_3O_4 nanoparticles in hydrophobic sol-gel materials. On the other hand, a novel tyrosinase biosensor based on Fe_3O_4 nanoparticles–chitosan nanocomposite has also been developed for the detection of phenolic compounds [10].

Prussian blue (PB), an inorganic conductor with Zeolite structure, attracts much interest of investigation especially for catalytic utilities since the first report on its synthesis by Neff [11–13]. Zhao reported that Fe_3O_4 nanoparticles modified with PB synthesized by chemical method were immobilized on the electrode surface by the casting technique and displayed catalysis to the reduction of H_2O_2 [14, 15]. However, the manual cast technique employed may result in its easy leach from the electrode surface, thus making it unstable.

To conquer this, a novel approach for electrochemically synthesizing core-shell Fe_3O_4-PB is provided using two steps of deposition in this article. The nano-Fe_3O_4 is firstly deposited on the glassy carbon electrode (GCE) surface forming a nano-Fe_3O_4/GCE. Then, the PB cover layer is electrochemically in situ deposited on the nano-Fe_3O_4 surface forming the core-shell structure. The properties of the Fe_3O_4-PB nanoparticles are characterized by cyclic voltammetry (CV), electrochemical impedance spectroscopy

J. Chumming (✉) · L. Xiangqin
Department of Chemistry,
University of Science and Technology of China,
Hefei 230026, China
e-mail: jcm@fudan.edu.cn

J. Chumming
Department of Chemistry, Fudan University,
Shanghai 200433, China

(EIS), superconducting quantum interference device (SQUID), and Fourier transmission infrared (FTIR) spectra. It was verified that the obtained core-shell Fe_3O_4-PB modified electrode has strong electrocatalytic activity toward H_2O_2 reduction. This is a continuation and deepening of our previous work on the role of the Fe_3O_4 nanoparticles in the fields of magnetite biosensors [6, 7].

Experimental

Materials

Iron powder reduced, ferric chloride, potassium ferricyanide, and H_2O_2 were purchased from Shanghai Reagents. All other reagents were of analytical grade and used without further purification. H_2O_2 solution was freshly prepared before each use. A 0.1 mol/l phosphate buffer solution (PBS) was prepared by mixing proper volumes of 1.0 mol/L K_2HPO_4 and 1.0 mol/L KH_2PO_4 stock solutions and adjusted with 1.0 mol/L H_3PO_4 and 1.0 mol/L KOH. Doubly distilled water was used to prepare all solutions. High-purity nitrogen was used for solution deaeration and a nitrogen atmosphere in the cell was kept during the experiments.

Apparatus and procedure

Electrochemical experiments such as CV and amperometric *i–t* curve were performed on a model CHI832 electrochemistry analyzer (Chen-Hua, Shanghai, China). EIS measurements were carried out at a CHI 660A workstation (Chen-Hua). All electrochemical experiments employed a three-electrode system, which consisted of a working electrode, a platinum wire auxiliary electrode and a saturated calomel reference electrode (SCE). All potentials in the paper were reported vs SCE. A GCE (Φ= 4 mm) or Al foil (2×1 cm) was used as the basal electrode for modification. Experiments were carried out at room temperature.

X-ray diffraction (XRD) was recorded on a MXPAHF rotating anode X-ray diffractometer (Japan) with a Cu-K_α radiation resource (λ=1.54056 Å) in the 2θ range from 20° to 70°.

The morphology image of the PB-Fe_3O_4/GCE surface was obtained on JSM-6700F field emission scanning electron microanalyzer (FE-SEM; JEOL, Japan).

EIS measurements were carried out in 0.01 mol/L Fe$(CN)_6^{4-/3-}$+0.1 mol/L KCl in the range of 100 kHz to 0.05 Hz at 0.2 V, the formal potential of the Fe$(CN)_6^{4-/3-}$ redox couple.

The DC magnetic measurements of Fe_3O_4 and PB-Fe_3O_4 deposited on Al foil were performed using Magnetic Properties Measurement System quantum design SQUID magnetometer.

FTIR spectra were obtained by using model Vector 22 FTIR spectrometer (Bruker, Germany).

Preparation of nano-Fe_3O_4

The nano-Fe_3O_4 particles were prepared via chemical co-precipitation according to the reported method [16]. $FeCl_3 \cdot 6H_2O$ (1.1 g, 4 mmol) and 0.03 g Fe (0.5 mmol) were dissolved in 100 ml of deoxygenated water. A concentrated $NH_3 \cdot H_2O$ solution in minor excess was added drop by drop to the solution under mechanical stirring until the pH reaches 10 at 80°. Thereafter, the crystal growth was allowed to proceed at 80° for 1 h. A dark precipitate was then isolated from the suspension by centrifugation decantation, washed with deoxygenated water, until the pH of the suspension solution reached 7.0. The purified Fe_3O_4 particles were then obtained.

XRD spectrum can be used for nano-particle analysis [17, 18]. The XRD result of the synthesized Fe_3O_4 particles is shown in Fig. 1. In the range 20–70°, six major peak at 2θ value of 30.3°, 35.5°, 43.3°, 53.7°, 57.2°, and 62.8° were observed, which was indexed as (2 2 0), (3 1 1), (4 0 0), (4 2 2), (5 1 1), and (4 4 0) directions, respectively. From these diffraction data, it could be inferred that the spinel structure Fe_3O_4 has been synthesized [18]. According to Scherrer's equation, $\beta=\kappa\lambda/D\cos\theta$, where λ is the X-ray wavelength, κ, the shape factor (0.89), D, the average diameter of the crystals in angstroms, θ, the Bragg angle in degree, and β is the line broadening measured by half-height in radium. When the reflection peak at 2θ of 35.5° was used, an averaged diameter of the Fe_3O_4 particles was calculated as 12 nm.

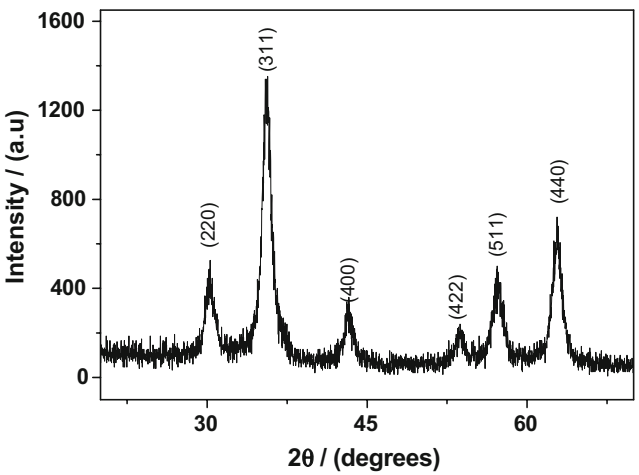

Fig. 1 XRD spectrum of the synthesized nano-Fe_3O_4

Fabrication of nano-Fe_3O_4/GCE and PB-Fe_3O_4/GCE

Prior to modification, the bare GCE was polished successively with 3, 1, and 0.05 μm α-alumnia slurry on a polishing pad. Then, it was rinsed with water and sonicated in water and ethanol for 5 min, respectively. Finally, it was dried under a nitrogen flow and ready for use.

The nano-Fe_3O_4 (40 mg) was dispersed in 10 ml anhydrous alcohol under sonication for use. A 5-μL aliquot of this dispersion was dropped onto the surface of GCE and dried in the air, forming the nano-Fe_3O_4 particles modified electrode, denoted as nano-Fe_3O_4/GCE.

The nano-Fe_3O_4/GCE was cycled scanning at a scan rate of 50 mV/s between −0.2 and 1.2 V in a fresh solution containing 5×10^{-3} mol/L $K_3[Fe(CN)_6]$+0.1 mol/L pH 2.0 PBS for ten cycles. The obtained modified electrode was labeled as PB-Fe_3O_4/GCE.

The illustration of the PB-Fe_3O_4 core-shell configuration is expressed in Scheme 1.

Results and discussion

Voltammetric fabrication of PB-Fe_3O_4

Figure 2 shows the CVs of the nano-Fe_3O_4/GCE in 5×10^{-3} mol/L $K_3[Fe(CN)_6]$+0.1 mol/L pH 2.0 PBS at 50 mV/s. Two typical pairs of redox peaks were growing up at E_m ($E_m=E_{pa}/2+E_{pc}/2$) of 0.21 V (I) and 0.89 V (II), which can be attributed to the redox reactions of PB/Prussian white and PB/Prussian green, respectively. Comparatively, the bare GCE shows only a redox couple at E_m of about 0.28 V for $Fe(CN)_6^{3-}/Fe(CN)_6^{4-}$ reaction, and nano-Fe_3O_4/GCE does not show any peaks in 0.1 mol/L pH 2.0 PBS.

Since the isoelectric point of Fe_3O_4 is about 6.5 [19], the surface charge of the nano-Fe_3O_4 should be positive in 0.1 mol/L pH 2.0 PBS. Attachment of negatively charged $Fe(CN)_6^{3-/4-}$ on the surface of nano-Fe_3O_4 can be expected, which is favorable to the formation of $Fe[Fe(CN)_6]^{-n}$ (n=0–2) structured layer by providing $Fe^{3+/2+}$ cations. This led to the formation of the core-shell PB-Fe_3O_4. Experiments showed that the ten-cycle scan is suitable for the formation of the core-shell PB-Fe_3O_4. In addition, the morphology of the nano-Fe_3O_4/GCE after scans is shown in Fig. 3; it can be seen that the surface is covered by the PB-Fe_3O_4 nanoparticles of 50–120 nm size.

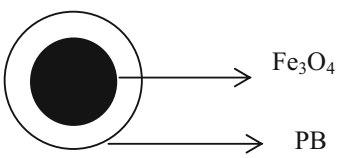

Scheme 1 The core-shell configuration of the PB-Fe_3O_4

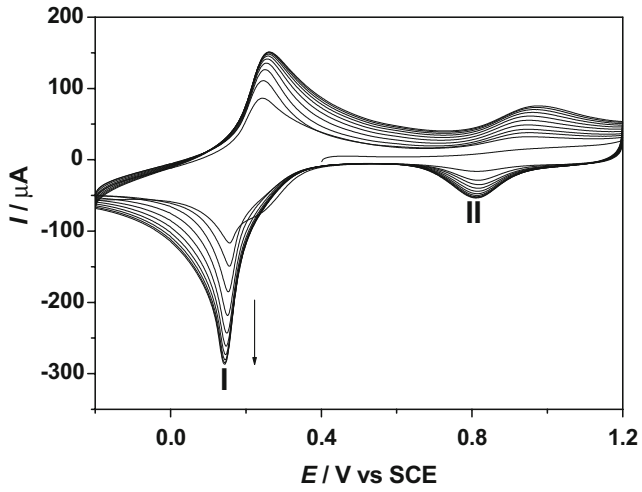

Fig. 2 CVs of the nano-Fe_3O_4/GCE in 5×10^{-3} mol/L $K_3[Fe(CN)_6]$+0.1 mol/L pH 2.0 PBS. Scan rate, 50 mV/s

EIS for PB-Fe_3O_4/GCE

EIS is an effective method for evaluating the surface layer properties using the redox probe $Fe(CN)_6^{4-/3-}$ [20]. The total impedance of the electrode is determined by several parameters: solution resistance, R_{sol}; double layer capacitance, C_{dl}; charge transfer resistance, R_{ct}; and Warburg impedance, Z_w. In the actual circuit, the constant phase angle element (CPE) is used in place of pure capacitance considering the influence of the electrode surface roughness. CPE manifests itself by altering the expected shape of ideal capacitor/resistor combinations and is expressed as $Z(\mathrm{CPE})=A(j\omega)^{-n}$, where A and n ($0<n\leq1$) are frequency independent proportionality constants. When n=1, the CPE can be expressed as pure capacitance. The Randles equivalent circuit (Fig. 3, inset) comprising the R_{sol}, R_{ct}, Z_w, and CPE was used to fit the measured results of the nano-Fe_3O_4/GCE and PB-Fe_3O_4/GCE [21].

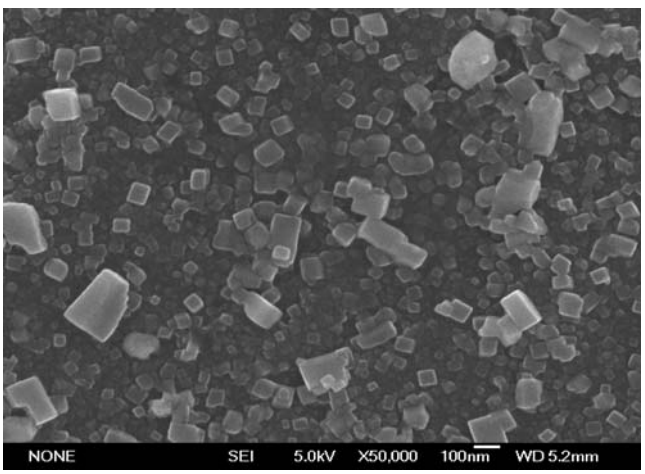

Fig. 3 FE-SEM image of PB-Fe_3O_4/GCE

The EIS results for the bare GCE (a), nano-Fe_3O_4/GCE (b), and PB-Fe_3O_4/GCE (c) in 0.01 mol/L $Fe(CN)_6^{4-/3-}$+ 0.1 mol/L KCl solution are shown in Fig. 4. From Fig. 4, it can be seen that Fig. 4a shows a small semicircle domain of 112.5 Ω in diameter with an almost straight tail line, which is characteristic of a diffusion limiting step of the electrochemical process [22–24]. Figure 4b displays much higher interfacial R_{ct}, the semicircle is significantly enlarged, and an R_{ct} value of 820.3 Ω can be calculated. These results indicate that the negative Fe_3O_4 nanoparticles layer forms a significant blocking effect of the $Fe(CN)_6^{4-/3-}$ redox reaction in 0.1 mol/L KCl solution. However, the semicircle is reduced a little bit on the PB-Fe_3O_4/GCE, as shown in Fig. 4c, and an R_{ct} value of 687.6 Ω can also be calculated. The reduction of the R_{ct} value suggests that the PB-Fe_3O_4 nanoparticles accelerate the $Fe(CN)_6^{4-/3-}$ redox reaction compared with the nano-Fe_3O_4, and the PB has been attached to the nano-Fe_3O_4 surface. Moreover, it can be seen that these fitted curves are in well consistent with the experimental results.

Magnetic properties of the PB-Fe_3O_4

The magnetic properties of nano-Fe_3O_4 (a) and PB-Fe_3O_4 (b) on Al foil were measured at the room temperature (298 K) and demonstrated in Fig. 5, respectively. The typical superparamagnetic behavior is observed by showing almost immeasurable coercivity and remanence, which is also the characteristic property of the magnetite. For pure Fe_3O_4 (a), the saturation magnetization (Ms) is 60 emu/g, which is less than that of the bulk magnetite [25]. The difference may be attributed to the small particle size effect. For PB-Fe_3O_4 (b), the Ms reduced to 18 emu/g probably mainly owing to the shielding effect of the PB layer on the Fe_3O_4 surface, also demonstrating that the Fe_3O_4 nanoparticles have been entrapped in the PB film.

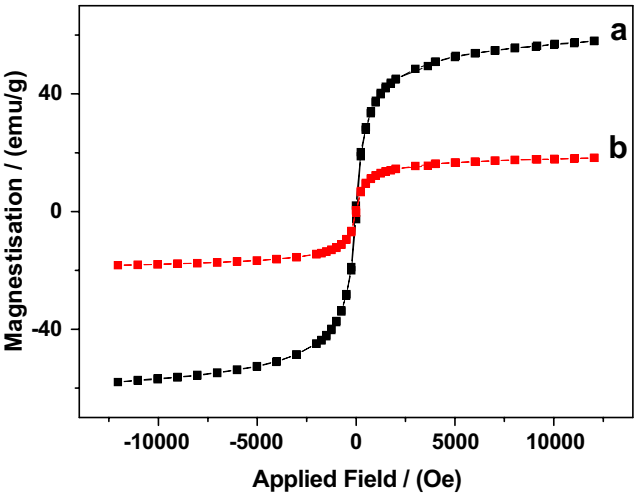

Fig. 5 Magnetization loops for Fe_3O_4 (**a**) and PB-Fe_3O_4 (**b**) deposited on Al foil

FTIR spectra for PB-Fe_3O_4

Figure 6 shows the FTIR spectra of the synthesized nano-Fe_3O_4 (a) and the PB-Fe_3O_4 (b). The characteristic absorption band at about 580.3 cm^{-1} is attributed to the stretching of Fe–O bond [26]. In addition, the absorption bands near 3,421.5 and 1,624.8 cm^{-1} refer to the O–H stretching mode and H–O–H bending mode [27], respectively, indicating the presence of certain amount of interstitial water in these samples. A new band at 2,081.8 cm^{-1} appeared at the curve a is characteristic of PB, which corresponds to the stretching vibration of the Fe (III)–CN–Fe(II) structure [28]. These results also indicate the formation of PB-Fe_3O_4 with core-shell structure.

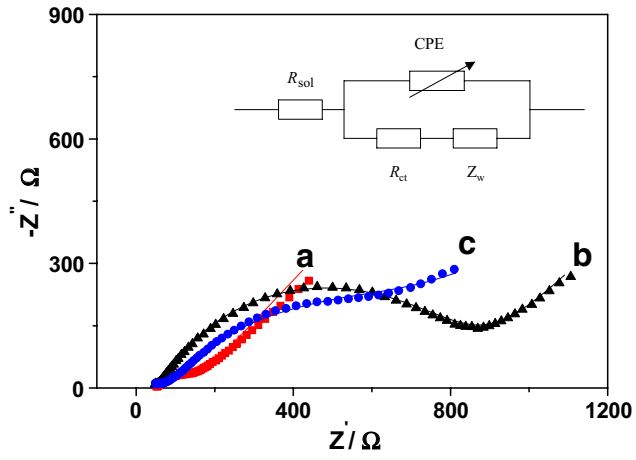

Fig. 4 EIS results of the bare GCE (**a**), nano-Fe_3O_4/GCE (**b**), and PB-Fe_3O_4/GCE (**c**) in 0.01 mol/L $Fe(CN)_6^{4-/3-}$+0.1 mol/L KCl at 0.2 V between 100 kHz and 0.05 Hz

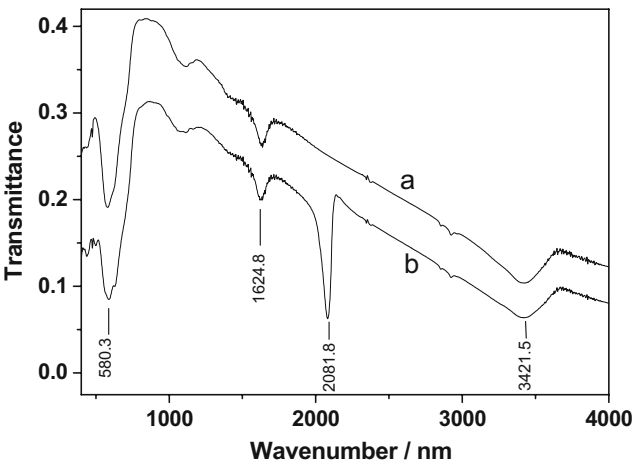

Fig. 6 FTIR spectra of the synthesized nano-Fe_3O_4 (**a**) and PB-Fe_3O_4 (**b**)

Electrochemical behavior of the PB-Fe_3O_4/GCE

The electrochemical behavior of the PB-Fe_3O_4/GCE in 0.1 mol/L pH 6.0 PBS at different scan rates was investigated. As shown in Fig. 7, the redox peak currents of couple (I) are both proportional to the square root of the scan rate from 20 to 200 mV/s, indicating a diffusion controlled redox process. Here, it is important to note that, indeed, only the diffusion of K^+ in the PB lattice [29]. The surface concentration of the PB (Γ_0*) can be calculated based on the equation $Q=nFA\Gamma_0$* (where F is Faraday constant, Q can be obtained by using the reduction peak current of couple, I, on the assumption that the surface roughness of the GCE was 10 after the nano-Fe_3O_4 deposition on the electrode surface, n and A stand for the number of electron transferred and the geometrical surface area of the electrode, respectively) [30]. Therefore, Γ_0* is approximately 1.09×10^{-10} mol/cm^2, showing a monolayer modification.

The influence of pH on the electrochemical behavior of the PB-Fe_3O_4/GCE was also studied. With increasing the pH value from 2.0 to 10.0, the redox peak potentials of couple (I and II) were almost unchanged, while the peak currents gradually decreased. This can be explained by the fact that the PB is not very stable in neutral and alkaline solution, and Prussian White is somewhat solvable in water [15].

Electrocatalytic reduction toward H_2O_2 on the PB-Fe_3O_4/GCE

Figure 8 shows the CVs of the PB-Fe_3O_4/GCE in 0.1 mol/L pH 6.0 PBS in the absence (a) and presence (b) of 2×10^{-3} mol/L H_2O_2. From the Fig. 8a, it can be observed that the signal of redox couple (I) from PB layer appeared. With the addition of 2×10^{-3} mol/L H_2O_2, as shown in Fig. 8b, the reduction current of couple (I) increased significantly accompanied by the decrease of the oxidation current, indicating an electrocatalytic effect toward the reduction of H_2O_2. As is well known, Fe_3O_4 nanoparticles have no catalytic activity to H_2O_2 reduction.

According to this phenomena, an electrolysis potential was selected at −0.05 V for obtaining a higher sensitivity of amperometric measurements. Figure 9 shows a typical steady state amperometric i–t response of the PB-Fe_3O_4/GCE to the successive addition of 2×10^{-4} mol/L H_2O_2 into 0.1 mol/L pH 6.0 PBS under stirring. A stepped increase of H_2O_2 concentration caused a corresponding stepped growth

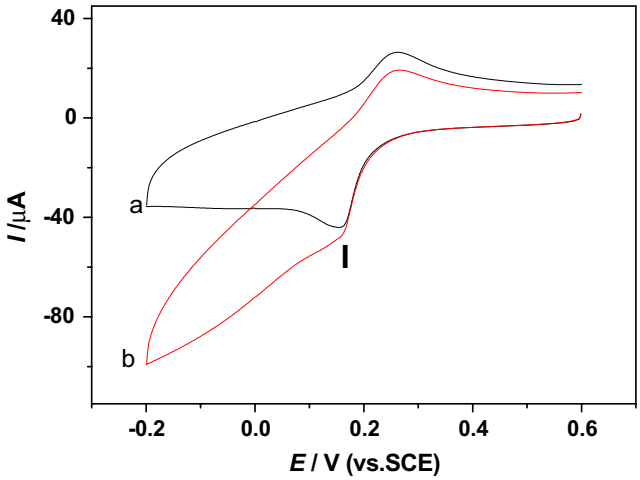

Fig. 8 CVs of the PB-Fe_3O_4/GCE in 0.1 mol/L pH 6.0 PBS solution in the absence (**a**) and presence (**b**) of 2×10^{-3} mol/L H_2O_2. Scan rate, 50 mV/s

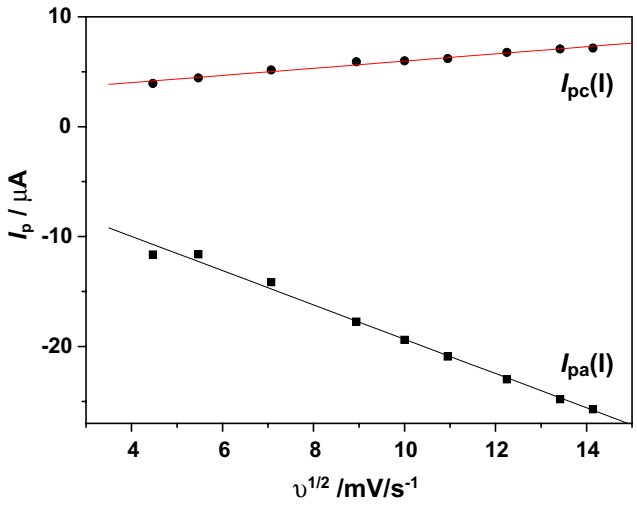

Fig. 7 The linear relationship between the redox peak currents of couple (I) with the square root of scan rate from 20 to 200 mV/s in 0.1 mol/L pH 6.0 PBS solution

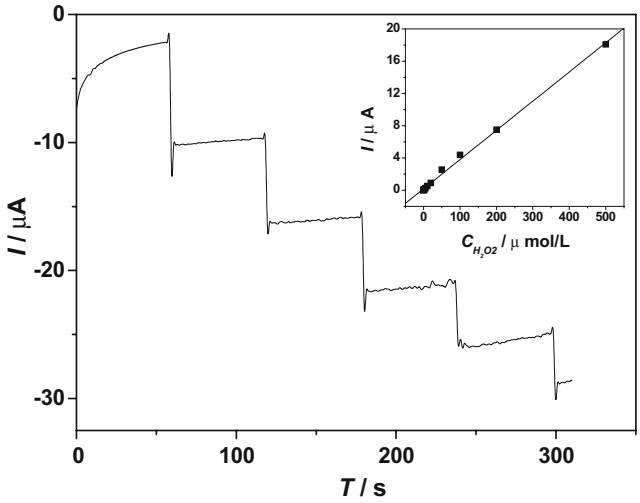

Fig. 9 Amperometric i–t response of the PB-Fe_3O_4/GCE to the successive addition of 2×10^{-4} mol/L H_2O_2 into 0.1 mol/L pH 6.0 PBS under stirring at −0.05 V. *Insert* Plot of catalytic current vs H_2O_2 concentration

of reduction currents. Moreover, after each addition of 2×10^{-4} mol/L H_2O_2, the modified electrode responded rapidly within 3 s to reach the steady state. The nearly equal currents steps for each addition of H_2O_2 demonstrate a stable and efficient electrocatalytic property of the PB-Fe_3O_4/GCE, and the electrocatalytic ability is three times larger than that of the protein-Fe_3O_4 films [5]. By using amperometric *i–t* curve technique, a linear relationship between the reduction current (I) and the concentration of H_2O_2 (C_{H2O2}) was obtained in the concentration range of 1×10^{-7}~5×10^{-4} mol/L with a linear regression equation of I (μA)=0.1811+0.0362 C_{H2O2} (μmol/L) (r=0.9987), as shown in Fig. 9 insert, which was also more boarder than that previously reported in the literature [31]. A detection limit of 2×10^{-8} (s/n=3) was determined. Using the Lineweaver–Burk plot, the apparent Michaelis–Menten constant (K_m), which is an indication of the enzyme-substrate kinetics, can be calculated. The K_m value for the horseradish peroxidase/DNA/GCE is estimated to be 0.83×10^{-3} mol/L.

Reproducibility and stability

The reproducibility of the current response of the PB-Fe_3O_4/GCE was examined in the presence of 2×10^{-4} mol/L H_2O_2 in 0.1 mol/L pH 6.0 PBS. The relative standard deviation for ten repeat injections was 2.4%.

The stability of the PB-Fe_3O_4/GCE was also examined. Almost no change of the current response was found for a week during its storage in 0.1 mol/L pH 6.0 PBS at 4 °C, and only about 12% for 1 month. Above experimental data demonstrated that the PB-Fe_3O_4/GCE has good stability and long lifetime.

Conclusions

In this work, the Fe_3O_4-PB nanoparticles with core-shell structure were in situ fabricated by electrochemically depositing PB on a nano-Fe_3O_4 modified GCE. It based on the excellent electrocatalytic property of the PB and on the good biocompatibility of the Fe_3O_4 displays significant electrocatalytic activity to the reduction of H_2O_2. Hence, this provides an alternate way for the determination of H_2O_2 and especially shows a new applicable prospect for Fe_3O_4 nanoparticles in fabricating magnetite biosensors. Moreover, the metal substituted analogues of PB with the core-shell structure can also be synthesized by using this method. Further investigations are in progress now.

Acknowledgment We gratefully acknowledge the financial support from the Specialized Research Fund for the Doctoral Program of Higher Education (no. 20040358021) and National Natural Science Foundation of China (no. 20575062).

References

1. Mosbach K, Andersson L (1977) Nature 2701:259 doi:10.1038/270259a0
2. Pinho MS, Gregori ML, Nunes RCR, Soares BG (2001) Poym Degrad Stab 73:1 doi:10.1016/S0141-3910(00)00198-1
3. Katz E, Weizmann H, Willner I (2005) J Am Chem Soc 1271:9191
4. Cheng GF, Zhao J, Tu YH, He PG, Fang YZ (2005) Anal Chim Acta 5331:11 doi:10.1016/j.aca.2004.10.044
5. Cao DF, He PL, Hu NF (2003) Analyst (Lond) 128:1268 doi:10.1039/b308242c
6. Gong JM, Lin XQ (2003) Chin J Chem 21:761
7. Gong JM, Lin XQ (2003) Microchem J 75:51 doi:10.1016/S0026-265X(03)00053-5
8. Yang HH, Zhang SQ, Chen XL, Zhuang ZX, Xu JG, Wang XR (2004) Anal Chem 76:1316 doi:10.1021/ac034920m
9. Reetz MT, Zonta A, Vijayakrishnan V, Schimossek K (1998) J Mol Catal Chem 134:251 doi:10.1016/S1381-1169(98)00043-0
10. Wang SF, Tan YM, Zhao DM, Liu GD (2008) Biosens Bioelectron 23:1781 doi:10.1016/j.bios.2008.02.014
11. Ding Y, Gu G, Xia XH (2008) J Solid State Electrochem 12:553 doi:10.1007/s10008-007-0342-0
12. Neff VD (1978) J Electrochem Soc 125:886 doi:10.1149/1.2131575
13. Zhang D, Wang K, Sun DC, Xia XH, Chen HY (2003) J Solid State Electrochem 7:561 doi:10.1007/s10008-003-0420-x
14. Zhao G, Xu JJ, Chen HY (2006) Electrochem Commun 81:148 doi:10.1016/j.elecom.2005.11.001
15. Zhao G, Zhang QL, Li SP, Chen HY (2005) Chem Mater 17:3154 doi:10.1021/cm048078s
16. Hou YD, Li DZ, Zhang A, Fu XZ (2003) Chinese J Inorg Mater 18:929
17. Berger P, Adelman NB, Beckman KJ, Campbell DJ, Ellis AB, Lisensky GC (1999) J Chem Educ 76:943
18. Wang CY, Zhu GM, Chen ZY, Lin ZG (2002) Mater Res Bull 37:2525 doi:10.1016/S0025-5408(01)00787-5
19. Regazzoni AE, Urrutia GA, Blesa MA, Maroto AJG (1981) J Inorg Nucl Chem 431:489
20. Saby C, Oritz B, Champagne GY, Belanger D (1997) Langmuir 13:6805 doi:10.1021/la961033o
21. Bord AJ, Faulkner LR (1980) Electrochemical methods. Wiley, New Work, p 316
22. Ivnitski D, Willkins E, Tien HT, Ottova A (2000) Electrochem Commun 2:457 doi:10.1016/S1388-2481(00)00060-6
23. Ren XM, Pickup PG (1997) J Electroanal Chem 420:251 doi:10.1016/S0022-0728(96)04784-5
24. Lu LP, Wang SQ, Lin XQ (2004) Anal Chim Acta 519:161 doi:10.1016/j.aca.2004.05.062
25. Zaitsev VS, Filimonov DS, Presnyakov IA, Gambino RJ, Chu B (1999) J Colloid Interface Sci 212l:49 doi:10.1006/jcis.1998.5993
26. Waldron RD (1995) Phys Rev 99:1727 doi:10.1103/Phys-Rev.99.1727
27. Ayers JB, Piggs WH (1971) J Inorg Nucl Chem 33:721 doi:10.1016/0022–1902(71)80470-0
28. Itaya K, Uchida I, Neff VD (1970) Acc Chem Res 9:2512
29. Zakharchuk NF, Meyer B, Hennig H, Scholz F, Jaworsi A, Stojek Z (1995) J Electroanal Chem 398:23 doi:10.1016/0022-0728(95)04225-2
30. Laviron E (1979) J Electroanal Chem 100:263 doi:10.1016/S0022-0728(79)80167-9
31. Tsenga KS, Chena LC, Hoa KC (2005) Sensors Actuators B 108l:738